ELSEVIER

Contents lists available at ScienceDirect

# Journal of Membrane Science

journal homepage: www.elsevier.com/locate/memsci



# Blood oxygenation artificial lung membranes – three incremental modification strategies to improve hemocompatibility

Bao Tran Duy Nguyen <sup>a,1</sup>, Yea Eun Hahm <sup>b,1</sup>, Bich Phuong Nguyen Thi <sup>b</sup>, Seung Hwan Kim <sup>a</sup>, Guntak Song <sup>b</sup>, Zhuomin Jiang <sup>c,d</sup>, Mukhammad Kayumov <sup>e</sup>, Dowan Kim <sup>f</sup>, In-Seok Jeong <sup>f</sup>, Kangwon Lee <sup>c,d,\*</sup>, Yeong Don Park <sup>b,\*\*</sup>, Jeong F. Kim <sup>a,\*\*\*</sup>

- <sup>a</sup> Department of Chemical Engineering, Kyung Hee University, Yongin, 17104, Republic of Korea
- <sup>b</sup> Department of Energy and Chemical Engineering, Incheon National University, Incheon, Republic of Korea
- c Department of Applied Bioengineering, Graduate School of Convergence Science and Technology, Seoul National University, Seoul, 08826, Republic of Korea
- d Research Institute for Convergence Science, Seoul National University, Suwon-si, Gyeonggi-do, Republic of Korea
- e Division of Transplant Surgery, Department of Surgery, Brigham and Women's Hospital, Harvard Medical School, Boston, MA, USA

# ARTICLE INFO

#### Keywords: Blood oxygenation Artificial lung Hemocompatibility Artificial organ Blood repellent surface

#### ABSTRACT

The primary challenge in membrane-based artificial lung technology is the limited hemocompatibility, which often leads to thrombosis and hemolysis, threatening the patient's life. Ironically, despite safety concerns over perfluoroalkyl substances (PFAS), fluorochemicals exhibit irreplaceable amphiphobicity, resulting in superb long-term hemocompatibility. Therefore, for biomedical applications, it is important to impartially assess the toxicity of PFAS over short-term PFAS exposure for life-threatening situations. In this study, three incremental surface modification strategies—superhydrophobic, superamphiphobic, and slippery liquid-infused porous surface (SLIPS) coatings-were developed and systematically compared to enhance hemocompatibility without compromising oxygenation performance. Superhydrophobic modification onto cellulose acetate membranes provided improved blood repellency but was insufficient in mitigating protein adsorption and long-term coagulation. Superamphiphobic membranes, modified via perfluoroalkylsilane coatings on nanostructured surfaces, exhibited enhanced resistance to both aqueous and lipid fouling; the modification efficacy strongly depended on the carbon chain lengths. SLIPS coating, consisting of a tethered perfluorinated solid layer infused with a mobile perfluorocarbon liquid (FDA-approved as an artificial blood substitute), demonstrated outstanding antifouling and thromboresistant characteristics. Moreover, an ex vivo test using a 0.05 m2 hollow fiber membrane module with a liquid-repellent coating demonstrated complete thrombus-free operation after circulation with porcine blood. These findings could provide a background dataset when assessing the advantages and disadvantages of PFAS for short-term medical intervention in life-threatening situations. Importantly, our data clearly conclude that PFAS-free SLIPS could be the optimal solution for next-generation artificial lung membranes.

#### 1. Introduction

Membrane technology has become an indispensable component in a wide range of applications, including water purification [1], organic solvent recovery [2,3], gas separation [4], batteries, and fuel cells [5]. In addition, membranes have found important applications in the

biomedical field since the early 20<sup>th</sup> century [6]. A notable example is hemodialysis using artificial kidney (AK) membranes, which dominates the blood purification market with an estimated value of USD 74 billion in 2019 [6]. In recent years, the emergence of COVID-19 and its associated respiratory complications has renewed attention for blood oxygenation artificial lung (AL) membranes, particularly in

f Department of Thoracic and Cardiovascular Surgery, Chonnam National University Hospital and Medical School, Gwangju, Republic of Korea

<sup>\*</sup> Corresponding author. Department of Applied Bioengineering, Graduate School of Convergence Science and Technology, Seoul National University, Seoul, 08826, Republic of Korea.

<sup>\*\*</sup> Corresponding author.

<sup>\*\*\*</sup> Corresponding author.

E-mail addresses: kangwonlee@snu.ac.kr (K. Lee), ydpark@inu.ac.kr (Y.D. Park), JeongKim@khu.ac.kr (J.F. Kim).

<sup>&</sup>lt;sup>1</sup> Bao Tran Duy Nguyen and Yea Eun Hahm contributed equally to this study.

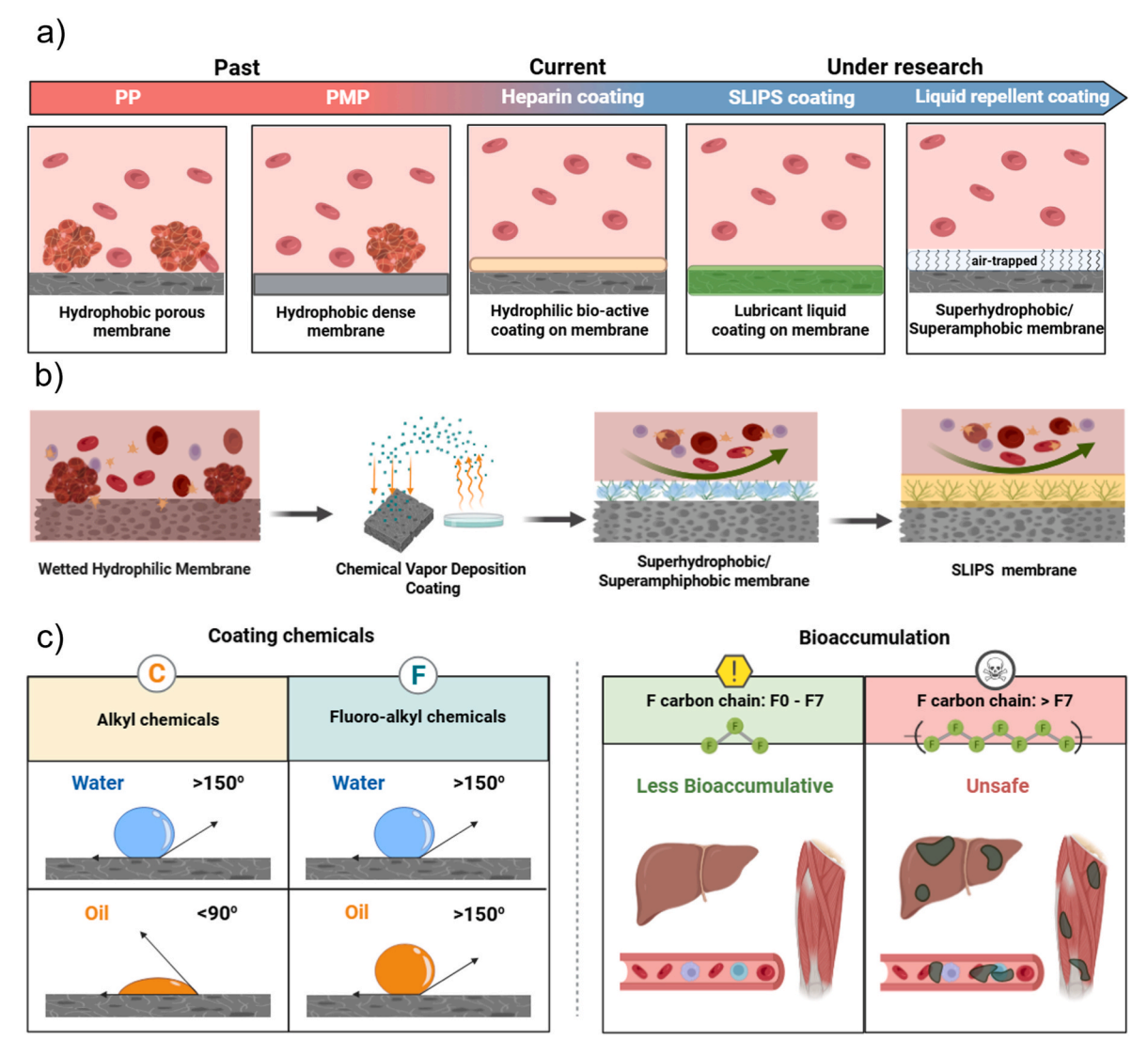


Fig. 1. (a) Artificial lung membrane materials from the past, current, and under research; (b) Use of Chemical Vapor Deposition method for liquid-repellent surface modifications; (c) Difference between alkyl and perfluoro-alkyl coating chemicals, and bioaccumulation of long-chain perfluoroalkyl chemicals.

extracorporeal membrane oxygenation (ECMO) devices for patients with acute lung failure [7].

Artificial lung (AL) devices operate as gas—liquid membrane contactors, where the membrane must remain non-wetted (i.e., dry) throughout operation. Blood flows on one side of the membrane, while a gas phase circulates on the opposite side. The membrane serves to physically separate the two phases while enabling the bidirectional exchange of oxygen and carbon dioxide between the gas and blood phases. To sustain efficient gas transfer, it is essential to prevent membrane wetting by blood, which necessitates the use of hydrophobic membrane materials. To fulfill this requirement, current AL membranes have employed polypropylene (PP) and polymethylpentene (PMP), respectively (Fig. 1(a)).

There are three main challenges in the current AL technology: (1) inadequate long-term hemocompatibility (leading to unwanted thrombosis and hemolysis), (2) excessive priming volume of the AL module (requiring large extracorporeal blood volume), and (3) suboptimal AL module design with poor mass transfer coefficients (permitting stagnant dead zones where blood coagulation initiates). These challenges are intricately interrelated and should preferably be solved simultaneously.

Among the challenges, the concept of hemocompatibility remains complex and multifactorial [8,9], with requirements varying significantly depending on the biomedical application (e.g., artificial kidneys,

artificial lungs, vascular stents). When the blood comes into contact with a foreign surface (e.g., membranes), the body's immune and coagulation pathways are rapidly activated. Within minutes, thrombus formation begins, resulting in the deposition of fibrin, red blood cells, platelets, and other blood components on the membrane surface.

Since the initial step in the blood coagulation cascade involves the adsorption of plasma proteins onto the biomaterial surface (e.g. membrane) [10], the primary objective of many studies on hemocompatibility has focused on reducing the surface protein adsorption through hydrophilic modification [11–13]. However, applying similar hydrophilic surface modifications to AL membranes can result in pore wetting and plasma leakage, ultimately reducing gas permeance and shortening membrane lifespan [14].

Therefore, a different strategy needs to be implemented on AL membranes. Instead of hydrophilic modification, we assert that superhydrophobic modifications could minimize the protein adsorption (thus enhanced hemocompatibility) while retaining the  $O_2/CO_2$  exchange efficiency. Superhydrophobic and superamphiphobic coatings have been reported to provide excellent anti-wetting performance along with reduced fouling by blood components [15–17].

Recently, SLIPS (Slippery Liquid-Infused Porous Surfaces) technology has emerged as an alternative strategy for enhancing hemocompatibility, involving a thin amphiphobic liquid layer immobilized on

porous substrates [18–20]. Interestingly, perfluorocarbon-based liquids have exceptionally high  $\rm O_2$  solubility, rendering them suitable for use as blood substitutes. Notably, Fluosol-DA (e.g., perfluorodecalin) was approved by the FDA as an artificial blood substitute in the 1980s [21]. This clinical precedent underscores the excellent biocompatibility of perfluorocarbons to be directly injected into the bloodstream [21].

To achieve effective blood-repellent surfaces, fluoroalkylsilane coatings have been widely employed, particularly in the design of SLIPS interfaces. However, there is a growing concern over the use of perfluoroalkyl substances (PFASs), evident in the recent European Chemicals Agency (ECHA) regulatory actions [22]. The adverse effects of PFAS are clear, but the fate of the EU PFAS regulation for biomedical applications remains uncertain, as the amphiphobic properties of fluorochemicals are practically irreplaceable in many biomedical devices, including artificial blood vessels (e.g., PTFE), stents, and membranes [23–25].

Completely replacing perfluorochemicals would be ideal, but the short-term use of perfluorocompounds should be carefully considered, gauging their advantages against potential toxicity. It is important to point out that the bioaccumulation tendency depends on the perfluorochemical length and structure. Although perfluorinated chemicals with eight or more carbon atoms (e.g., C8 and above) have been shown to bioaccumulate in living organisms [26], perfluorochemicals with less than eight carbon atoms have been shown to be removed by the liver [26] (Fig. 1(c)).

In this study, a comprehensive comparison of the three incremental surface modification strategies applied to blood oxygenation membranes—superhydrophobic, superamphiphobic, and slippery liquid-infused porous surface (SLIPS) coatings—was conducted, with a focus on the effects of varying fluorocarbon chain lengths. Cellulose acetate (CA)-based flat-sheet membranes were selected due to the scalability of CA in hollow fiber fabrication [27]. CA membranes were modified using three alkyltrichlorosilanes and three perfluoroalkyltrichlorosilanes to generate superhydrophobic and superamphiphobic surfaces. SLIPS coatings were then applied to the superamphiphobic samples to evaluate their combined performance in terms of hemocompatibility and gas exchange properties.

The hemocompatibility of the three modified membrane types was systematically evaluated through protein adsorption, whole blood adhesion, hemolysis, blood-repellent testing, cytotoxicity assays, and extended blood-contact studies. In parallel, their blood oxygenation performance—along with that of conventional PP and PMP membranes—was assessed using an *in vitro* oxygenation experiment with animal blood. By integrating the hemocompatibility data and gas exchange performance across different surface chemistries and chain lengths, this study could provide an important dataset to gauge the PFAS toxicity over its advantages objectively.

#### 2. Materials and experiment

# 2.1. Materials

The chemicals used for self-assembled monolayer (SAM) surface modifications included *n*-propyltrichlorosilane (C3), *n*-hexyltrichlorosilane (C6), *n*-octyltrichlorosilane (C8), *1H*,1*H*,2*H*,2*H*-perfluoropropyltrichlorosilane (F3), *1H*,1*H*,2*H*,2*H*-perfluorohexyltrichlorosilane (F6), and *1H*,1*H*,2*H*,2*H*-perfluorooctyltrichlorosilane (F8), all purchased from Gelest Inc. (USA). Krytox 101 was obtained from The Chemours Company (USA). Citrated and fibrinated sheep blood for oxygenation and hemocompatibility experiments was supplied by Kisan Bio Inc. (Republic of Korea). Gases (N2, CO2, O2) were provided by Joong-Ang Industrial Gas Inc. (Republic of Korea). Hexadecane (>99%), diiodomethane (>99%), ethylene glycol (>99%), cyclohexane (>99%), sodium dodecyl sulfate (SDS), glutaraldehyde solution (50 wt% in H2O), and phosphate-buffered saline (PBS, pH 7.4) were obtained from Sigma-Aldrich Korea. Ethanol (EtOH, 99.9%) was purchased from

Daejung Chemicals (Republic of Korea). Cellulose acetate (CA, 0.2  $\mu m$  pore size) and polypropylene (PP, 0.2  $\mu m$  pore size) membrane filters were purchased from GVS Filter Technology. O-rings were obtained from Allrubber® (Republic of Korea). The NanoOrange Protein Quantitation Kit was supplied by Thermo Fisher Scientific (Republic of Korea). Human umbilical vein endothelial cells (HUVECs) and EBM-2/EGM-2 BulletKit culture medium were purchased from Lonza. The (Poly(4-methyl-1-pentene)–PMP membrane was fabricated following our previous work [28].

#### 2.2. Surface modification

In this study, superamphiphobic membranes were prepared using short-chain, non-bioaccumulative perfluoroalkyl silanes (F3, F6) and a long-chain, bioaccumulative analog (F8) to evaluate their blood oxygenation performance. For comparison, superhydrophobic membranes were also fabricated using alkyltrichlorosilanes with similar carbon chain lengths (C3, C6, and C8) (see Table S1). All surface modifications were carried out via chemical vapor deposition (CVD), as illustrated in Fig. 1(b).

Cellulose acetate (CA) membranes (0.3 g) were placed in a glass chamber with 0.3 mL of silane chemical under vacuum (75 Torr) for 24 h. After CVD treatment, membranes were heat-cured at 120  $^{\circ}\text{C}$  for 1.5 h and subsequently washed with ethanol. The self-assembled monolayer (SAM) formation process and hydrolysis mechanism are illustrated in Fig. S1.

The superamphiphobic membranes (F3, F6, F8) were washed with ethanol and dried under nitrogen prior to use. SLIPS sample was prepared by drop-coating 15  $\mu$ L cm $^{-2}$  of Krytox 101 onto the F6-coated membrane.

#### 2.3. Characterization and performance evaluation

# 2.3.1. Characterization of modified membranes

The surface morphologies of the oxygenation membranes were examined using field-emission scanning electron microscopy (FE-SEM; JSM-7800F, JEOL, Japan). Surface roughness was analyzed by atomic force microscopy (AFM; Dimension 3100, Bruker, USA). Chemical compositions were characterized by attenuated total reflectance Fourier-transform infrared spectroscopy (ATR-FTIR; Nicolet 6700, Thermo Scientific, USA) and X-ray photoelectron spectroscopy (XPS; PHI 5000 VersaProbe II, ULVAC-PHI, Japan). The static water contact angles and surface energy were measured using a contact angle goniometer (Theta Lite, Biolin Scientific, Sweden).

# 2.3.2. Wetting stability test

The wetting stability of the PP, PMP, superhydrophobic (C3, C6, C8), and superamphiphobic (F3, F6, F8) membranes was evaluated by measuring the liquid entry pressure (LEP). After 24 h of immersion in deionized (DI) water, one side of the membrane was exposed to water, while the opposite side remained in contact with air in a dead-end test cell. Water pressure was increased in 0.5 bar increments every 30 min until water breakthrough was observed. The LEP value was recorded as the pressure at which the first water droplet penetrated through the membrane.

#### 2.3.3. Gas permeance test

The gas permeance of the membranes was evaluated using a deadend test cell under a transmembrane pressure of 1.0 bar. Air,  $O_2$ , and  $CO_2$  gases were individually applied to the membrane, and the resulting gas flow rates were measured. Permeance values were reported in Gas Permeation Units (GPU), where 1 GPU =  $10^{-6}$  cm<sup>3</sup>(STP)·cm<sup>-2</sup>·s<sup>-1</sup>·cmHg<sup>-1</sup>.

# 2.3.4. Silane coating durability

The durability of the silane coating was assessed using a water-jet

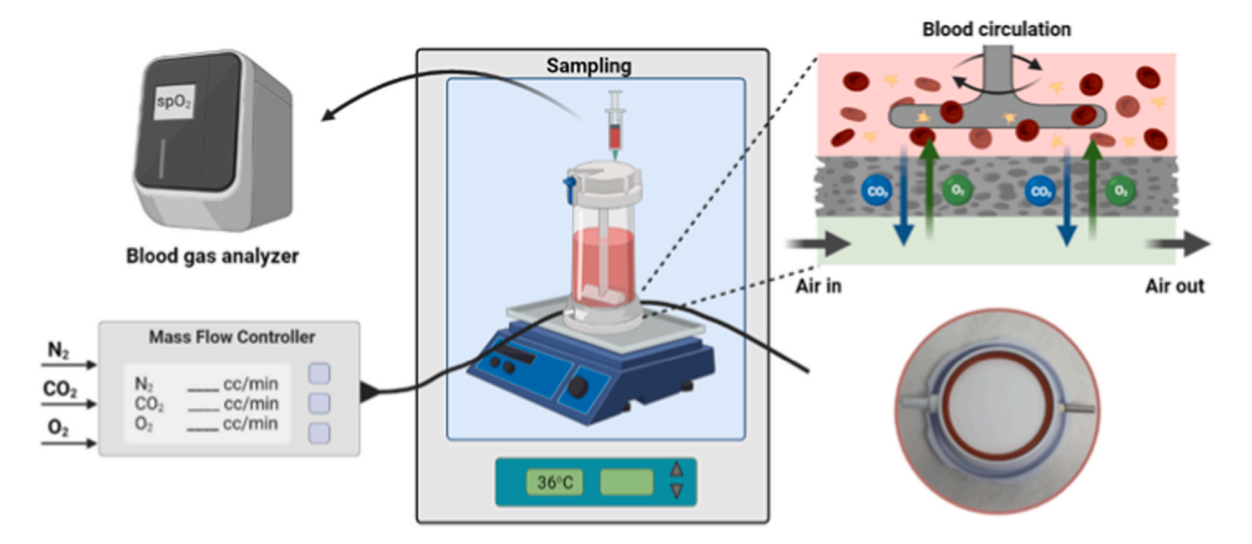


Fig. 2. Blood oxygenation dead-end cell apparatus schematic.

stability test. A total of 30 L of water was applied at a flow rate of 0.5 L  $\min^{-1}$  from a height of 45 cm onto the membrane, which was fixed at a 30° tilt. After exposure, the water contact angle was measured to evaluate the stability and retention of the silane coating.

#### 2.3.5. Membrane blood oxygenation performance

The blood oxygenation performance of the fabricated membranes was evaluated using a lab-scale dead-end membrane oxygenator (Fig. 2). Sheep blood (composition detailed in Table S2) was first deoxygenated by purging a gas mixture of  $N_2$ :CO<sub>2</sub> (10:1) through the gas side of the membrane (diameter = 4.25 cm). On the blood-contacting side, the blood was continuously stirred at 400 rpm using a touchless magnetic stirrer to enhance mass transfer (Fig. S2). Once the blood oxygen saturation dropped below 70 %, pure  $O_2$  was introduced into the gas side at a flow rate of 500 cc·min<sup>-1</sup> to initiate oxygenation.

All experiments were conducted in an incubator maintained at 36 °C. The change in blood oxygen concentration was measured using a blood gas analyzer (i-Smart300, i-SENS Inc., Republic of Korea). The oxygen transfer rate (mL  $O_2 \cdot m^{-2} \cdot \min^{-1}$ ) was calculated by dividing the total amount of oxygen transferred (mL  $O_2$ ) by the membrane's effective blood-contacting area (m²). The total  $O_2$  transferred included both oxygen bound to hemoglobin ( $hbO_2$ ), and dissolved oxygen in plasma ( $plO_2$ ) [29]. The bound  $O_2$  was determined from the hemoglobin concentration ( $C_{Hb}$ ,  $g \cdot L^{-1}$ ) and oxygen saturation (SO<sub>2</sub>, %), using the  $O_2$  carrying capacity of hemoglobin (1.39, mL  $O_2 \cdot g^{-1}$ ). The dissolved  $O_2$  was calculated from the partial pressure of oxygen (PO<sub>2</sub>, mmHg) and the solubility coefficient (0.0314, mL ·mmHg $^{-1} \cdot L^{-1}$ ). The blood volume  $V_{blood\ (L)}$  represented the total blood volume used in the experiemnt.

#### h.

Following incubation, unbound protein was removed by triple rinsing with PBS. The membranes were transferred to a fresh 24-well plate, secured with new O-rings, and incubated with 1 mL ethanol at 37 °C for 30 min to desorb adsorbed proteins. The eluates were evaporated to dryness at 50 °C, after which 350  $\mu L$  of NanoOrange® working solution (500  $\times$  dye dilution, prepared according to the manufacturer's instructions [30]) was added. Samples were protected from light, vortex-mixed, heated to 96 °C for 10 min, cooled to room temperature, and vortexed again to ensure homogeneity. To avoid particulate interference, solutions were filtered prior to fluorescence measurement.

Fluorescence intensity was measured in 200  $\mu$ L aliquots using a SpectraMax M2 microplate reader (Molecular Devices, USA) with excitation/emission wavelengths of 485/595 nm, an emission cutoff of 570 nm, and 20 flashes per read with automatic integration time. BSA calibration curves (10 ng mL<sup>-1</sup> to 10  $\mu$ g mL<sup>-1</sup>) in NanoOrange working solution were used to calculate the protein mass adsorbed. The final protein adsorption value was normalized to the membrane surface area exposed to the protein solution (1.09 cm<sup>2</sup>).

#### 2.3.7. Whole blood adhesion and coagulation test

Membrane samples (15 mm diameter) were placed into a 24-well plate secured with O-rings and incubated with 1 mL of citrated sheep whole blood (Kisanbio Inc.) at 37  $^{\circ}$ C under gentle shaking (100 rpm) for 24 h.

After incubation, the samples were prepared for SEM analysis to evaluate blood adhesion and coagulation. The samples were fixed in 4 % glutaraldehyde overnight at 4  $^{\circ}$ C, then rinsed three times with phosphate-buffered saline (PBS, pH 7.4). Following fixation, the mem-

$$O_2 \text{ transfer rate } \left(\frac{\textit{mL } O_2}{\textit{min} \cdot \textit{m}^2}\right) = \frac{\textit{hb} O_2 + \textit{pl} O_2}{\textit{dt} \cdot \textit{A}} = \frac{\left[\left(\% S_{O_2 \textit{out}} - \% S_{O_2 \textit{in}}\right) \cdot C_{\textit{Hb}} \cdot 1.39 \right. \\ \left. + \left(P_{O_2 \textit{out}} - P_{O_2 \textit{in}}\right) \cdot 0.0314\right] \cdot V_{\textit{blood}}}{\textit{dt} \cdot \textit{A}} \tag{1}$$

#### 2.3.6. Protein adsorption evaluation

The protein adsorption of the membranes was assessed using bovine serum albumin (BSA) as a model protein. Membrane samples (diameter: 15 mm) were first rinsed in deionized water for 10 min along with Orings. Each sample was then placed in a 24-well plate fitted with O-rings and incubated with 1 mL of BSA/PBS solution (1 mg mL $^{-1}$ ) at 37 °C for 2

branes were dehydrated through a graded ethanol series (50 %, 70 %, 90 %, and 100 %) and dried under a stream of dry air before SEM analysis.

#### 2.3.8. Hemolysis test

Pristine and modified membrane samples were cut into  $1\times 1$  cm pieces and incubated in 1.5 mL of phosphate-buffered saline (PBS) at 37  $^{\circ}\text{C}$  for 2 h. Meanwhile, defibrinated sheep blood was centrifuged at

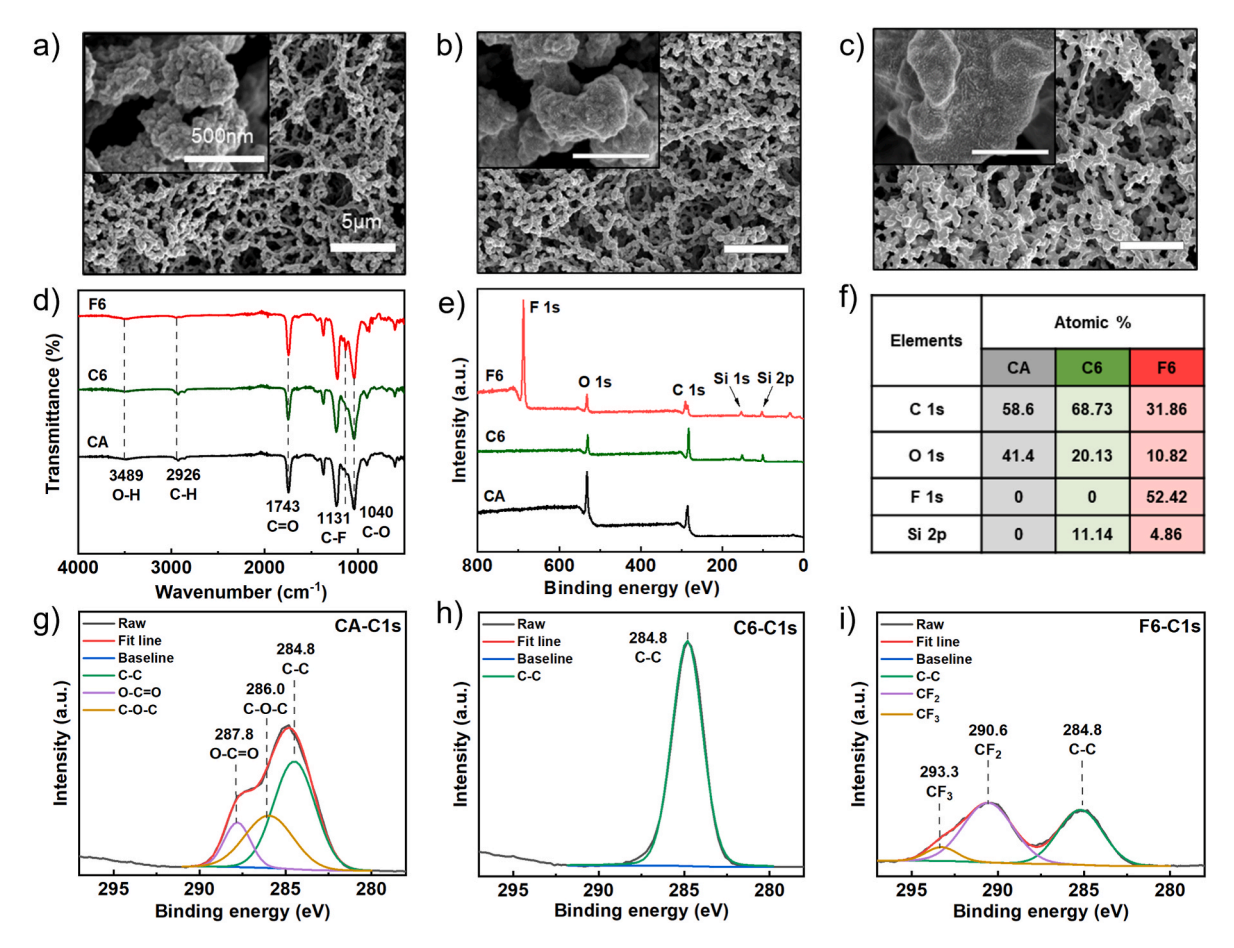


Fig. 3. Surface morphologies of (a) CA, (b) C6, and (c) F6. (d) FT-IR ATR spectra of CA, C6, F6. (e), (f), (g), (h), (i) XPS spectra and atomic percent of CA, C6, and F6 samples.

150 rpm for 10 min to isolate red blood cells (RBCs). After the initial incubation, 30  $\mu L$  of the isolated RBCs was added to each PBS-containing sample and further incubated at 37  $^{\circ}C$  for 2 h.

Following incubation, the solutions were centrifuged at 2500 rpm for 30 min to separate the supernatant. The absorbance of the supernatant was measured at 545 nm using a UV–Vis spectrophotometer (Genesys 150, Thermo Scientific). PBS and deionized water were used as negative and positive controls, respectively. The hemolysis rate (%) was calculated as follows:

Hemolysis rate 
$$\% = \frac{SA - SN}{SP - SN} X 100\%$$
 (2)

where SA is the sample absorption value, SN and SP are the negative and positive control absorption values.

# 2.3.9. Blood-repellent ability test and the long-term blood contacting test

The blood-repellent ability was evaluated by placing a drop of animal blood onto membranes tilted at a 30° angle and observing the interaction of the blood with the membrane surface. For the long-term blood contacting test, membranes and O-rings were washed sequentially with deionized water and ethanol, then dried under a clean bench environment. The membranes were then placed in a 6-well cell culture plate with O-rings, and 3 mL of defibrinated sheep blood was added to each well. For SLIPS-coated samples, Krytox 101 was applied prior to blood addition. The plates were sealed and stored at 5 °C for 14 days. After the incubation period, membranes were washed three times with phosphate-buffered saline (PBS) before further analysis.

# 2.3.10. Cytotoxicity

The cytotoxicity of membrane modifications was evaluated using the Cell Counting Kit-8 (CCK-8) assay to determine the viability of Human Umbilical Vein Endothelial Cells (HUVEC) after direct contact with the membranes. Cell cytotoxicity is inversely proportional to the measured cell viability percentage. Membrane samples (5  $\times$  5 mm<sup>2</sup>) were sterilized under UV light for 90 min and equilibrated in phosphate-buffered saline (PBS) for 1 h, repeated three times. HUVECs were seeded at a density of  $1 \times 10^4$  cells per well in a 96-well plate and incubated overnight. The culture medium was then replaced with fresh antibioticfree endothelial basal medium (EBM-2, Lonza). Prepared membrane samples were placed into the wells and incubated at 37 °C with 5 % CO<sub>2</sub> for 24, 48, and 72 h. Wells without membrane samples served as blank controls at each time point. Prior to measurement, samples and culture medium were removed, and 110 µL of fresh medium containing 10 % CCK-8 solution was added to each well and incubated for 45 min. Absorbance was measured at 450 nm using a microplate reader (BioTek Synergy H1 Hybrid Multi-Mode Reader, Agilent Technologies, USA). Cell viability was calculated by:

$$Cell~Viability~(\%) = \left[ \left( A_{sample} \right) - \left( A_{blank} \right) / \left( A_{Control} \right) - \left( A_{blank} \right) \right] \times 100\% \tag{3}$$

# 2.3.11. Ex vivo evaluation of a liquid-repellent hollow fiber membrane oxygenator module

Cellulose acetate (CA) hollow fibers were fabricated via a dry-jet wet spinning process using a dope solution of 21 wt% cellulose triacetate (CTA, Eastman Chemical Co., USA) and 79 wt% diluent. The solution was extruded through a spinneret under 0.5 bar bore fluid pressure, with zero air gap to ensure immediate phase inversion. Fibers were wound at

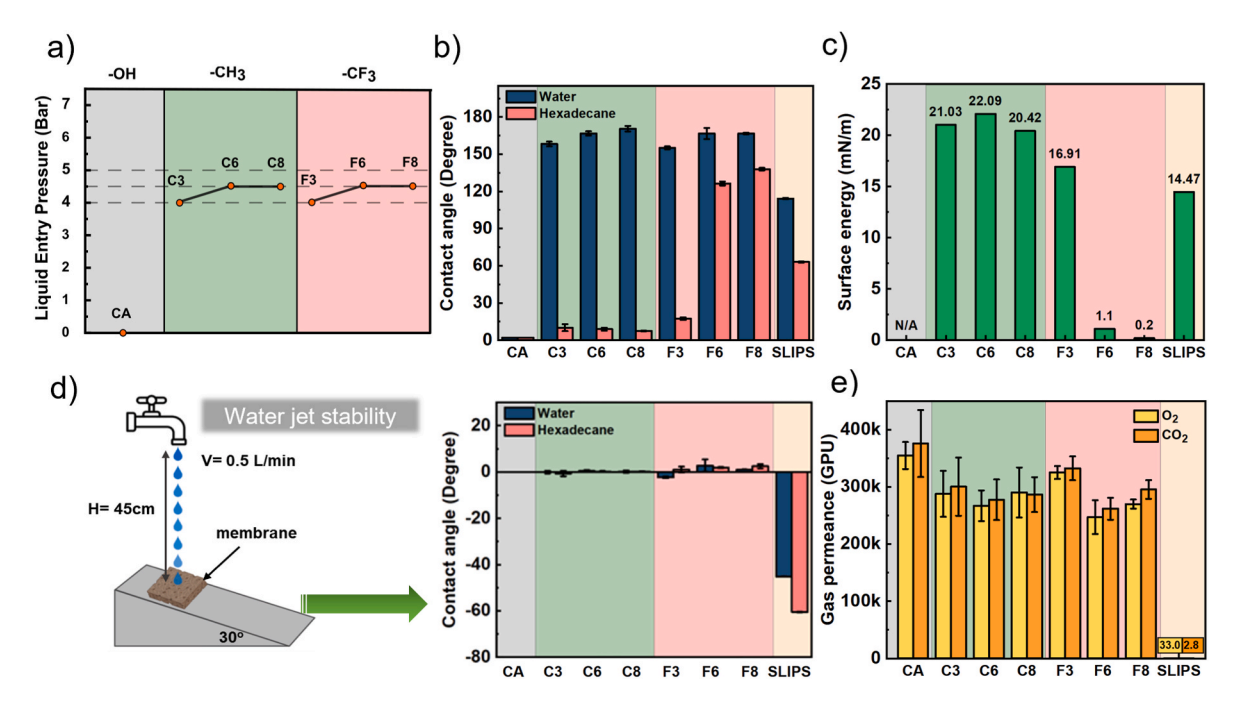


Fig. 4. The comparison of (a) liquid entry pressure (LEP) of the CA and the surface-modified membranes (LEP of PP and PMP membranes in this work were 2.0 bar and 7.5 bar, respectively); (b), (c) the contact angle and surface energy; (d) the water-jet stability scheme and contact angle decrease graph after the stability test; (e)  $O_2$  and  $CO_2$  gas permeance of all the samples.

70 m min<sup>-1</sup>, yielding uniform wall thickness and consistent morphology.

CA hollow fibers were subsequently coated with the F6 compound using a controlled chemical vapor deposition (CVD) process to confer liquid-repellent properties without altering fiber morphology. The coated fibers were assembled into a cylindrical oxygenator module with a total effective membrane area of 0.05  $\mbox{\em m}^2$ .

For performance evaluation, fresh venous blood (40 mL) was collected from a healthy male pig (22 kg) under systemic heparin anticoagulation. The oxygenator was incorporated into a closed-loop circulation circuit and driven by a peristaltic pump at 100 rpm. The feed oxygen was delivered to the gas side at a flow rate of 800 mL min<sup>-1</sup>. The experiment was conducted under a circuit pressure of 96/49 mmHg.

## 3. Results & discussion

In this study, the blood oxygenation performance of superamphiphobic membranes was evaluated using short-chain, non-bio-accumulative perfluoroalkyl chemicals (F3, F6) and a long-chain, bioaccumulative compound (F8). To compare effects at identical carbon chain lengths, superhydrophobic membranes were modified with corresponding alkyl silane chemicals C3, C6, and C8 (Table S1).

Surface morphology of the pristine cellulose acetate (CA) membrane (Fig. 3(a)) and CA membranes coated with alkyl silane (Fig. 3(b)) and fluoroalkyl silane chemicals (Fig. 3(c)) was examined by scanning electron microscopy (SEM). Post-CVD coating, the nodular structure on the CA membrane exhibited increased thickness, indicating successful silane polymerization (additional SEM images in Fig. S3).

Chemical compositions of the C6 and F6 coated membranes was further analyzed by FT-IR ATR and XPS analyses (Fig. 3(d–e)). FT-IR spectra (Fig. 3(d)) showed characteristic CA membrane peaks including –OH (3489 cm<sup>-1</sup>), C–H (2926 cm<sup>-1</sup>), C—O (1743 cm<sup>-1</sup>), and C–O (1040 cm<sup>-1</sup>) in both pristine and coated samples. Due to overlap with C–O absorption, Si–O–C bonding (1000–1100 cm<sup>-1</sup>) was difficult to observe directly by FT-IR; however, the presence of C–F bonds was confirmed by a distinct peak at 1131 cm<sup>-1</sup> in the F6 spectrum (full FT-IR spectra are shown in Fig. S4).

XPS analysis (Fig. 3(e)) revealed silicon peaks at Si 1s (154.8 eV) and Si 2p (102.5 eV) in both C6 and F6 membranes, confirming the presence of silane coatings. The F6 sample also showed a strong perfluoroalkyl signal at the F 1s peak (686.7 eV). The C 1s spectra (Fig. 3(g)) of pristine CA showed peaks corresponding to O–C=O (287.8 eV), C–O–C (286.0 eV), and C–C (284.8 eV). In contrast, the C6 spectrum exhibited only a C–C peak at 284.8 eV, while the F6 spectrum displayed C–C (284.8 eV) and fluorinated carbon peaks  $CF_2$  (290.6 eV) and  $CF_3$  (293.3 eV) (Fig. 3 (h–i)). The XPS auger electron escape depth ( $\lambda$ ) at the C1s peak ( $\sim$ 300 eV) is approximately 2 nm. Thus, the absence of the acetate peaks can be reasonably interpreted as evidence that the coating thickness exceeds 2 nm, confirming that the silane coatings fully cover the CA membrane surface (full XPS spectra in Fig. S5).

Elemental composition from XPS (Fig. 3(f)) aligns closely with the expected chemical formulas for C6 ( $O_3SiC_6H_{13}$ ) and F6 ( $O_3SiC_6H_4F_9$ ) coatings (full elemental percentages in Table S3). Taken together, FT-IR and XPS results confirm successful coating of alkyl silane and perfluoroalkyl silane layers on the CA membrane surface, with a coating thickness exceeding 5 nm.

Fig. 4(a) demonstrates that silane surface functionalization significantly enhanced the liquid entry pressure (LEP) of cellulose acetate membranes compared to the unmodified control. An LEP of >2 bar is considered to be sufficient to prevent unwanted blood intrusion during operation. The improvement scaled with the alkyl chain length of the silane precursors — short-chain (C3) treatments yielded LEP values near 4 bar, while longer-chain (C6 and above) modifications further improved LEP to approximately 4.5 bar.

To assess interfacial repellency, we evaluated static contact angles and calculated surface energies (Fig. 4(b and c)). All silane-modified membranes—both alkyl- and perfluoroalkyl-based—exhibited superhydrophobicity, with water contact angles exceeding  $150^{\circ}$ . F6- and F8-functionalized membranes further demonstrated superamphiphobic behavior, achieving hexadecane contact angles above  $120^{\circ}$  and ultralow surface energies of  $\sim\!1.1$  and  $\sim\!0.2$  mN m $^{-1}$ , respectively. In contrast, alkyl-coated membranes, while still hydrophobic, retained significantly higher surface energies ( $\sim\!20$  mN m $^{-1}$ ).

Due to safety concerns regarding the persistence and

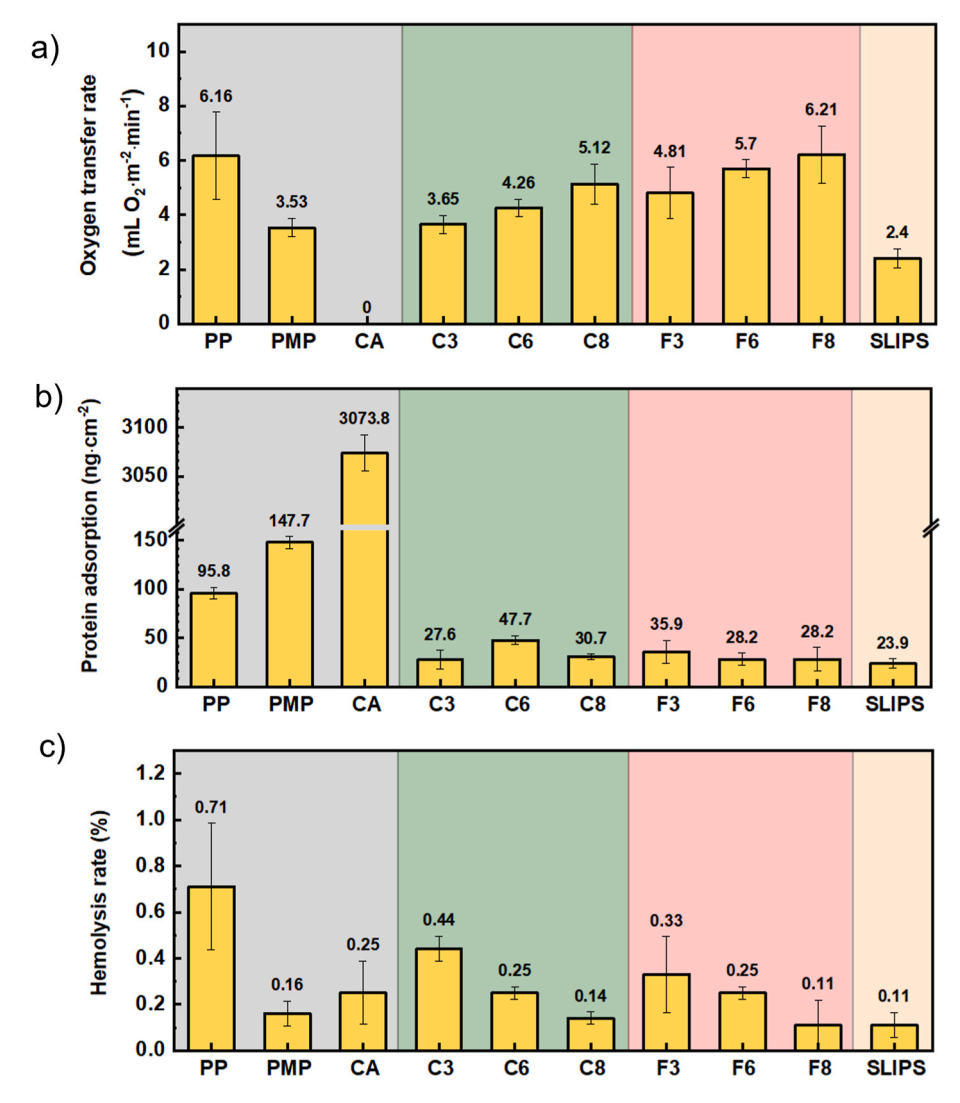


Fig. 5. (a) The oxygen transfer rate of all membrane samples using sheep blood, (b) albumin protein adsorption, and (c) hemolysis (%).

bioaccumulation potential of long-chain perfluorinated compounds, F6 was selected as the suboptimal candidate for subsequent SLIPS modification. A SLIPS layer was applied to the F6-coated membrane, resulting in a controlled increase in surface energy to 14.47 mN m $^{-1}$  and contact angles below  $120^{\circ}$  for both water and hexadecane—indicative of diminished surface repellency across polar and nonpolar interfaces.

Dynamic stability under fluid shear was evaluated using a water-jet test (Fig. 4(d)). While all silane-grafted membranes retained stable contact angles, the SLIPS-coated surface exhibited a measurable increase in wettability over time, trending toward the underlying F6 values. This behavior signifies lubricant loss under shear and highlights a key vulnerability of liquid-infused surfaces in physiologically relevant conditions.

Gas permeation measurements (Fig. 4(e)) revealed a slight reduction in  $O_2$  and  $CO_2$  permeance across all silane-treated membranes, attributed to marginal pore size contraction following vapor-phase grafting. Nevertheless, values remained above 250,000 GPU—well within the operational range for artificial lung applications. By contrast, the SLIPS membrane exhibited a pronounced decrease in gas permeance ( $O_2$ : 33 GPU;  $CO_2$ : 2.5 GPU), consistent with pore obstruction by the immobilized liquid layer. Importantly, this decrease did not impair oxygen transfer capacity (Fig. 5(a)), as the rate-limiting barrier in artificial lungs is governed by blood-side mass transfer resistance [6,31,32].

Fig. 5(a) presents the oxygen transfer rates of various membranes tested with sheep blood. The F6 and F8 membranes exhibited the highest

performance—5.7 and 6.21 mL  $O_2 \cdot m^{-2} \cdot min^{-1}$ , respectively—attributed to their low surface energy and high gas permeability. In contrast, the SLIPS-coated membrane, though possessing reduced gas permeance due to the liquid layer, sustained a reasonable oxygenation rate of 2.4 mL  $O_2 \cdot m^{-2} \cdot min^{-1}$ . This suggests that optimized hemocompatibility can partially compensate for limitations in gas diffusivity.

As shown in Fig. 5(b), protein adsorption was highest for conventional PP and PMP membranes (95.84 and 147.70 ng cm<sup>-2</sup>), consistent with their low antifouling capacity. The CA membrane, despite its hydrophilicity, displayed non-negligible adsorption due to its high wettability and surface interaction area. In contrast, all modified membranes demonstrated significantly lower protein adhesion. Among them, only the C8 surface approached the thrombogenic threshold of 30 ng cm<sup>-2</sup>, while F6, F8, and especially the SLIPS membrane remained well below it. The SLIPS surface recorded the lowest adsorption (23.9 ng cm<sup>-2</sup>), in line with minimal fouling and the absence of coagulated residues in Fig. 6(b).

Fig. 5(c) highlights the hemolysis profiles, with perfluorinated and SLIPS membranes demonstrating superior blood compatibility. Hemolysis decreased with increasing chain length, reaching minimum values for F8 and SLIPS, all falling below the critical 0.5 % threshold for clinical safety.

These findings emphasize that neither surface energy nor gas permeance alone governs membrane performance in blood-contacting applications. Instead, hemocompatibility arises from a multifactorial

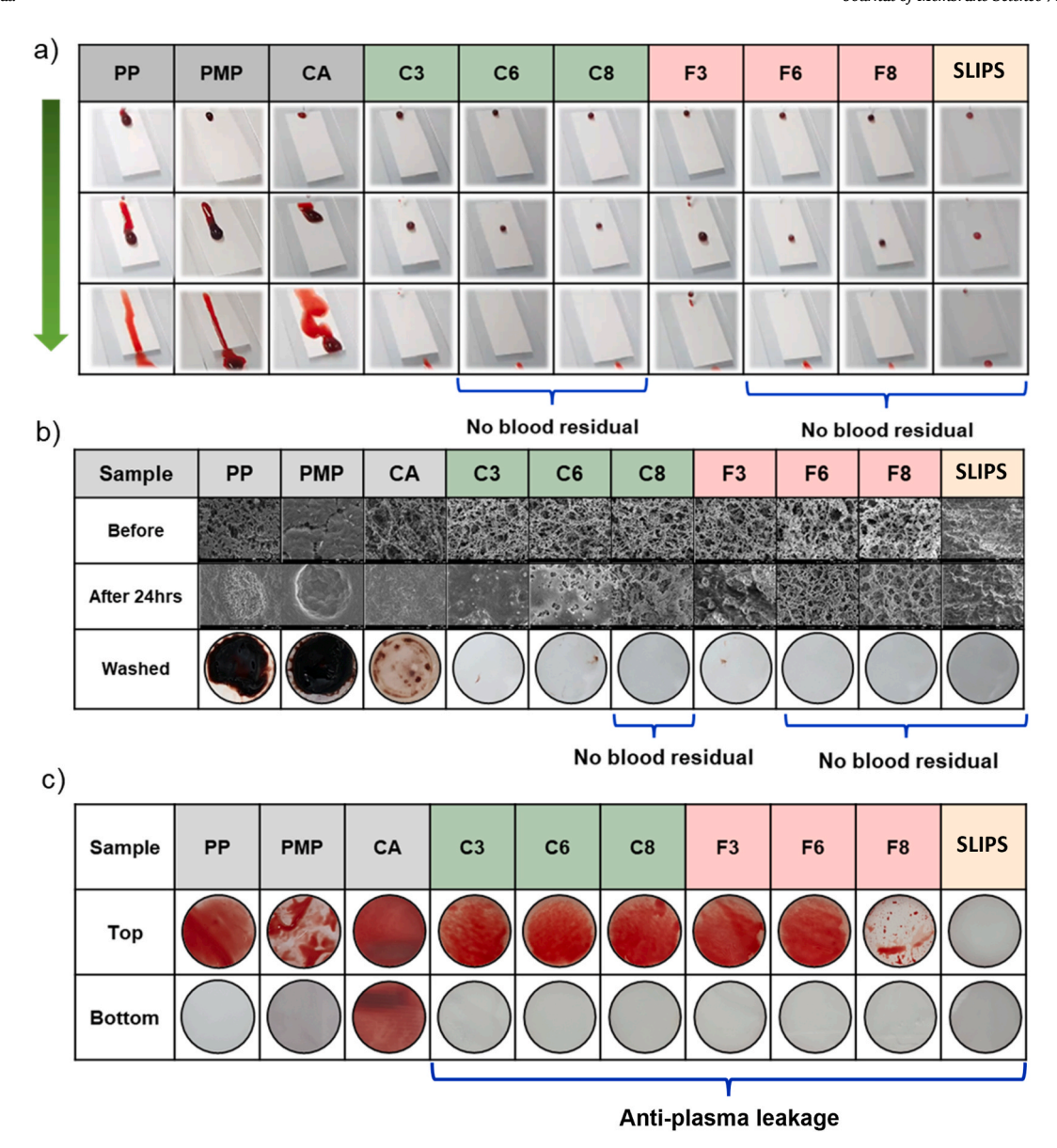


Fig. 6. (a) Photos of blood slides on the surface of the membranes, (b) the SEM images and photos of all samples before and after the whole blood coagulation in *in vitro* test at 37 °C for 24 h, and (c) photos of the top and the bottom surface of membranes after 14 days at 5 °C for testing the blood repellent stability.

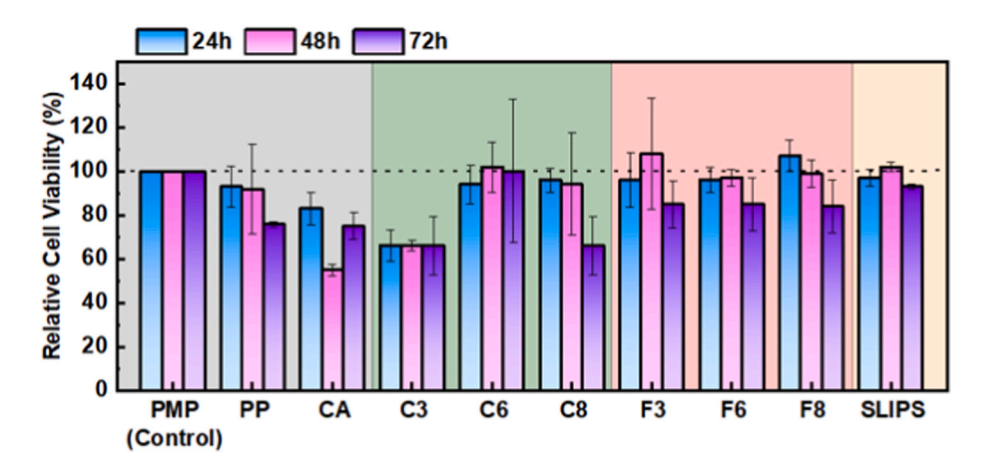
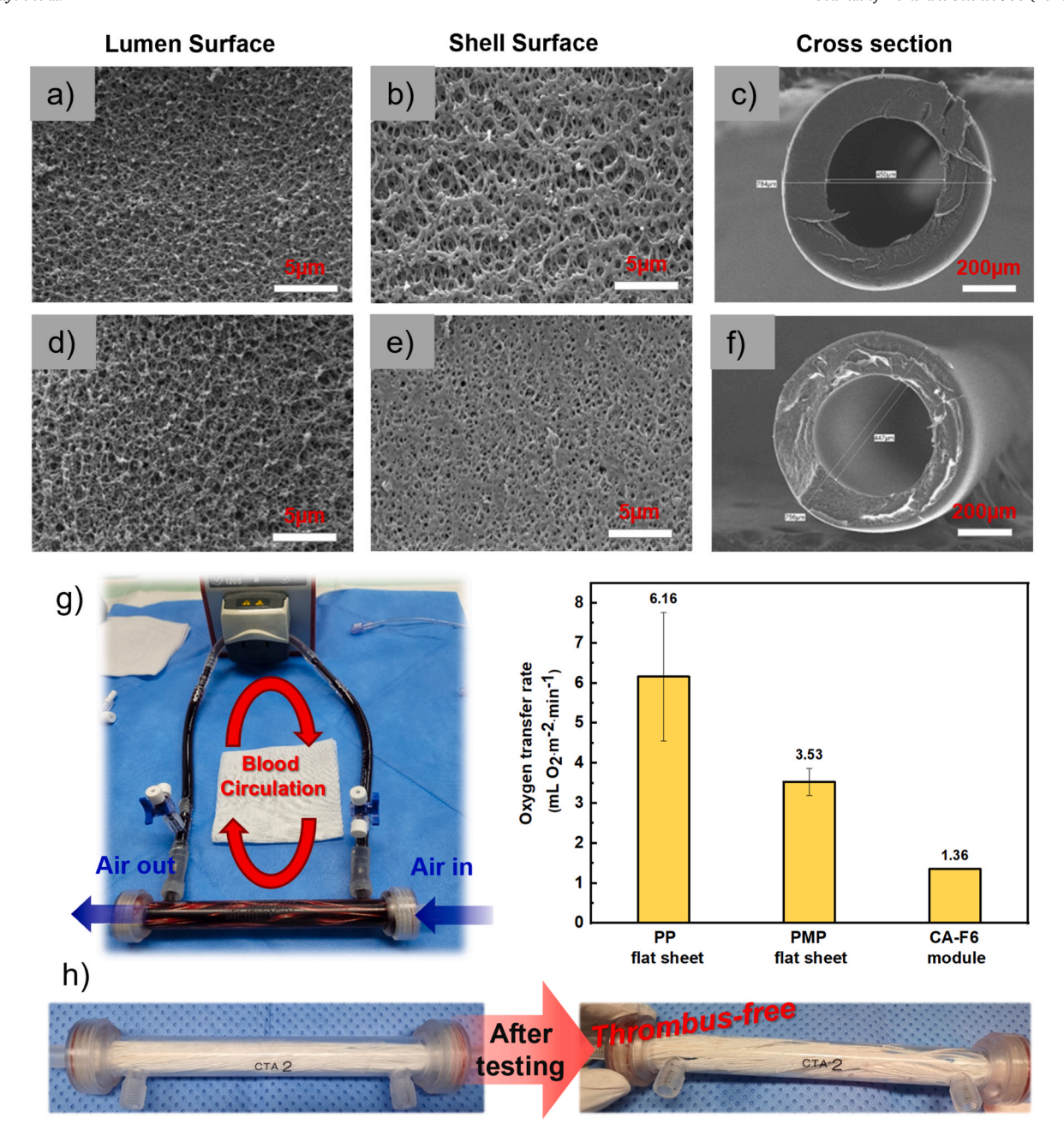


Fig. 7. Relative cell viability and cytotoxicity of PP, CA, and modified membranes assessed using the CCK-8 assay following ISO 10993–5:2009. Values are normalized to the PMP membrane, which was used as the control.



**Fig. 8.** SEM images of CA hollow fiber membranes: (a, b, c, d, e, f) lumen surfaces, shell surfaces, cross-sections of pristine and F6-coated membranes, respectively; (g) *Ex vivo* blood oxygenation test with a 0.05 m<sup>2</sup> CA hollow fiber F6 coated module; (h) CA hollow fiber F6 coated membrane before and after *ex vivo* test.

balance of interfacial chemistry, fouling resistance, and gas transport. To further validate long-term stability, all membranes underwent *in vitro* exposure under physiological conditions.

In Fig. 6(a), only the C6, C8, F6, F8, and SLIPS membranes showed no visible blood residue after static blood droplet testing, indicating effective blood repellency. In contrast, the short-chain samples, C3 and F3, exhibited inferior repellency, as evidenced by residual blood on the surface. The *in vitro* whole blood coagulation test (Fig. 6(b)) revealed a similar trend to the protein adsorption results: membranes such as C8, F6, F8, and SLIPS, all of which had protein adsorption levels below 30 ng cm<sup>-2</sup>, exhibited no visible blood clots after 24 h of contact. Conversely, the pristine PP, PMP, and CA membranes were entirely covered by blood clots, confirming their poor hemocompatibility.

The long-term blood exposure test further evaluated the durability of the surface coatings. While the superhydrophobic and superamphiphobic coatings (C6, C8, F6, and F8) initially repelled blood, they gradually lost this property after two weeks of static storage. This loss is attributed to the dissolution of air pockets within the surface textures upon prolonged contact with blood [16] (Video 1 in Supporting Information). Remarkably, the SLIPS-coated membrane maintained complete blood repellency even after 14 days under static conditions, as demonstrated in Video 2 (Supporting Information).

Overall, the SLIPS membrane exhibited excellent hemocompatibility, characterized by extremely low protein adsorption and sustained blood-repellent performance in *in vitro* tests. Furthermore, the SLIPS layer remained intact after 6 h of dynamic blood oxygenation testing (Video 3 in Supporting Information). It should be noted, however, that prior studies have reported that the SLIPS layer's integrity can be maintained for up to 72 h under dynamic *in vivo* conditions [18].

In Fig. 6(c), the bottom surfaces of the modified membranes from all three modification strategies exhibited no plasma leakage even after 14 days of contact with animal blood, whereas the hydrophilic pristine CA

membrane became fully wetted.

Because blood is in continuous contact with ECMO membranes and re-enters the patient's circulation over extended periods, it is essential to evaluate cytocompatibility. Relative cell viability was assessed at 24, 48, and 72 h, normalized to the PMP membrane as a control (Fig. 7), in accordance with ISO 10993–5:2009 standards [33]. A PMP membrane was used as the clinical benchmark due to its widespread adoption and established biocompatibility.

Across the first 48 h, membranes modified with longer alkyl (C6) and perfluoroalkyl (F6, F8) trichlorosilanes, as well as those incorporating a SLIPS layer, demonstrated equal or superior cytocompatibility relative to PMP. This trend suggests that low-surface-energy interfaces may mitigate protein fouling and cellular stress, promoting favorable interactions with HUVECs. At 72 h, a gradual decline in viability was observed across all membranes—including the PMP control—a pattern consistent with extended direct-contact exposure. Nonetheless, several modified surfaces (notably C6, F3, F6, F8, and SLIPS) retained high cell viability, indicating sustained cytocompatibility over clinically relevant durations. In contrast, the C3-coated membrane exhibited markedly reduced viability, highlighting the inadequacy of shorter chain lengths in establishing stable, bioinert surfaces. Collectively, these results underscore the advantage of superhydrophobic and superamphiphobic modifications—particularly those employing longer fluorinated chains or lubricant-infused architectures—in supporting endothelial cell viability over extended periods. Such properties are critical for nextgeneration artificial lung membranes intended for prolonged extracorporeal circulation.

Fig. 8 depicts the surface morphology and post–*ex vivo* performance of the F6-coated cellulose acetate (CA) hollow fiber membrane module. SEM analysis (Fig. 8(a–f)) confirms that the CVD-applied coating preserves the native structural integrity and smooth surface characteristics of the unmodified fibers, indicating no adverse morphological alteration.

The 0.05 m² membrane module demonstrated functional blood oxygenation capability during the  $ex\ vivo$  experiment (Fig. 8(g)). However, the oxygen transfer rate was limited (1.36 mL  $O_2 \cdot m^{-2} \cdot min^{-1}$ ), likely due to factors such as fiber packing density, arrangement, and flow path configuration. Following  $ex\ vivo$  blood circulation, visual inspection (Fig. 8(h)) revealed an absence of thrombus formation or clot adhesion, with the fiber bundle remaining visually clean and free from deposits. These findings highlight the liquid-repellent coating's resistance to thrombus formation under dynamic blood-contacting conditions, underscoring its potential suitability for advanced oxygenation devices, including ECMO applications.

# 4. Conclusions

In this study, three incremental surface modification strategies—superhydrophobic, superamphiphobic, and SLIPS—were systematically investigated for artificial lung membranes using alkyl and perfluoroalkyl trichlorosilanes of varying chain lengths to identify the optimal hemocompatible design. All strategies successfully enhanced hemocompatibility by reducing protein adsorption without introducing cytotoxic effects.

Both superhydrophobic and superamphiphobic modifications offered favorable performance, combining effective blood repellency with enhanced oxygenation. A positive correlation was observed between increasing alkyl/perfluoroalkyl chain length and improved surface properties, with a minimum effective chain length of six carbon atoms. While the superamphiphobic F6 membrane exhibited the best overall hemocompatibility, its long-term applicability may be constrained by PFAS restrictions. Nevertheless, the irreplaceable amphiphobicity of the fluorochemicals should be objectively evaluated in relation to their toxicity, particularly for short-term medical treatments. In contrast, the superhydrophobic modification could be employed as a viable and safer alternative, as the membrane hemocompatibility was

certainly superior to that of the commercial membranes (PP and PMP).

The SLIPS-coated membrane exhibited the best blood repellency and lowest protein adsorption, indicating superior hemocompatibility. However, liquid (oil) retention under dynamic blood flow conditions remains a challenge to be solved. Importantly, the performance superiority of the SLIPS coating clearly suggests that PFAS-free SLIPS could outperform the superamphiphobic modification, and it will be the aim of our future research.

#### CRediT authorship contribution statement

Bao Tran Duy Nguyen: Writing – review & editing, Writing – original draft, Visualization, Formal analysis, Data curation, Conceptualization. Yea Eun Hahm: Writing – original draft, Methodology, Conceptualization. Bich Phuong Nguyen Thi: Methodology, Formal analysis, Conceptualization. Seung Hwan Kim: Visualization, Formal analysis, Data curation. Guntak Song: Methodology, Formal analysis. Zhuomin Jiang: Resources, Methodology, Formal analysis. Mukhammad Kayumov: Methodology, Formal analysis, Data curation. Dowan Kim: Methodology, Formal analysis, Conceptualization. In-Seok Jeong: Methodology, Formal analysis, Data curation. Kangwon Lee: Writing – review & editing, Project administration, Investigation, Conceptualization. Yeong Don Park: Writing – review & editing, Project administration, Investigation, Conceptualization, Investigation, Conceptualization, Funding Agency & editing, Project administration, Investigation, Resources, Project administration, Investigation, Funding acquisition.

#### Declaration of competing interest

The authors declare that they have no known competing financial interests or personal relationships that could have appeared to influence the work reported in this paper.

#### Acknowledgments

This research was supported by Nano Material Technology Development Program (RS-2021-NR057370) and Basic Science Research Program (RS-2024-00394111) through the National Research Foundation of Korea funded by the Ministry of Science and ICT.

#### Appendix A. Supplementary data

Supplementary data to this article can be found online at https://doi.org/10.1016/j.memsci.2025.124858.

# Data availability

Data will be made available on request.

#### Data availability

Data will be made available on request.

#### References

- [1] Y. Liao, C.-H. Loh, M. Tian, R. Wang, A.G. Fane, Progress in electrospun polymeric nanofibrous membranes for water treatment: fabrication, modification and applications, Prog. Polym. Sci. 77 (2018) 69–94.
- [2] H.Y. Nguyen Thi, S. Kim, B.T. Duy Nguyen, D. Lim, S. Kumar, H. Lee, G. Szekely, J. F. Kim, Closing the sustainable life cycle loop of membrane technology via a cellulose biomass platform, ACS Sustain. Chem. Eng. 10 (7) (2022) 2532–2544.
- [3] W. Choi, C. Lee, D. Lee, Y.J. Won, G.W. Lee, M.G. Shin, B. Chun, T.-S. Kim, H.-D. Park, H.W. Jung, Sharkskin-mimetic desalination membranes with ultralow biofouling, J. Mater. Chem. A 6 (45) (2018) 23034–23045.
- [4] K. Xie, Q. Fu, G.G. Qiao, P.A. Webley, Recent progress on fabrication methods of polymeric thin film gas separation membranes for CO2 capture, J. Membr. Sci. 572 (2019) 38–60.
- [5] J.H. Kim, S.J. Moon, S.H. Park, M. Cook, A.G. Livingston, Y.M. Lee, A robust thin film composite membrane incorporating thermally rearranged polymer support for

- organic solvent nanofiltration and pressure retarded osmosis, J. Membr. Sci. 550 (2018) 322–331
- [6] B.T. Duy Nguyen, H.Y. Nguyen Thi, B.P. Nguyen Thi, D.-K. Kang, J.F. Kim, The roles of membrane technology in artificial organs: current challenges and perspectives, Membranes 11 (4) (2021) 239.
- [7] X. Hong, J. Xiong, Z. Feng, Y. Shi, Extracorporeal membrane oxygenation (ECMO): does it have a role in the treatment of severe COVID-19? Int. J. Infect. Dis. 94 (2020) 78–80.
- [8] B.D. Ratner, The Blood Compatibility Catastrophe, Wiley Online Library, 1993, pp. 283–287.
- [9] B.D. Ratner, The catastrophe revisited: blood compatibility in the 21st century, Biomaterials 28 (34) (2007) 5144–5147.
- [10] S.R. Hanson, E.I. Tucker, R.A. Latour, Blood coagulation and blood-material interactions, in: Biomaterials Science, Elsevier, 2020, pp. 801–812.
- [11] B.P.N. Thi, B.T.D. Nguyen, I.-S. Jeong, J.F. Kim, Hemocompatibility challenge of membrane oxygenator for artificial lung technology, Acta Biomater. (2022).
- [12] A. Mollahosseini, A. Abdelrasoul, A. Shoker, A critical review of recent advances in hemodialysis membranes hemocompatibility and guidelines for future development, Mater. Chem. Phys. 248 (2020) 122911.
- [13] R. Li, G. Wu, Y. Ye, In vitro hemocompatibility of sulfonated polypropylene nonwoven fabric prepared via a facile γ-ray pre-irradiation grafting method, Appl. Surf. Sci. 356 (2015) 1221–1228.
- [14] T. Yeager, S. Roy, Evolution of gas permeable membranes for extracorporeal membrane oxygenation, Artif. Organs 41 (8) (2017) 700–709.
- [15] A.C. Lima, J.F. Mano, Micro-/nano-structured superhydrophobic surfaces in the biomedical field: part I: basic concepts and biomimetic approaches, Nanomedicine 10 (1) (2015) 103–119.
- [16] V. Jokinen, E. Kankuri, S. Hoshian, S. Franssila, R.H. Ras, Superhydrophobic blood-repellent surfaces, Adv. Mater. 30 (24) (2018) 1705104.
- [17] J. Lv, Y. Cheng, Fluoropolymers in biomedical applications: state-of-the-art and future perspectives, Chem. Soc. Rev. 50 (9) (2021) 5435–5467.
- [18] T.R. Roberts, J.H. Choi, D.S. Wendorff, G.T. Harea, B.M. Beely, K.N. Sieck, M. E. Douglass, P. Singha, J.B. Dean, H. Handa, Tethered liquid perfluorocarbon coating for 72 hour heparin-free extracorporeal life support, ASAIO J. 67 (7) (2021) 798–808.
- [19] E. Lepowsky, S. Tasoglu, Emerging anti-fouling methods: towards reusability of 3D-printed devices for biomedical applications, Micromachines 9 (4) (2018) 196.
- [20] D.C. Leslie, A. Waterhouse, J.B. Berthet, T.M. Valentin, A.L. Watters, A. Jain, P. Kim, B.D. Hatton, A. Nedder, K. Donovan, A bioinspired omniphobic surface

- coating on medical devices prevents thrombosis and biofouling, Nat. Biotechnol. 32 (11) (2014) 1134–1140.
- [21] J.-H. Kim, E.-A. Jung, J.-E. Kim, Perfluorocarbon-based artificial oxygen carriers for red blood cell substitutes: considerations and direction of technology, Journal of Pharmaceutical Investigation 54 (3) (2024) 267–282.
- [22] ECHA, Annex XV Restriction Report: Proposal for a Restriction.
- [23] N. Famaey, J. Verhoeven, S. Jacobs, M. Pettinari, B. Meyns, In situ evolution of the mechanical properties of stretchable and non-stretchable ePTFE vascular grafts and adjacent native vessels, Int. J. Artif. Organs 37 (12) (2014) 900–910.
- [24] H. Wang, R. Xu, S. She, M. Abdullah, K. Meng, M. Xiao, J. Nie, H. Zhao, K.-Q. Zhang, PTFE stent membrane based on the electrospinning technique and its potential for replacing ePTFE, ACS Appl. Bio Mater. 7 (12) (2024) 8608–8620.
- [25] Q. Liya, G. Yanjie, W. Guoqing, X. Yihui, G. Dali, J. Chao, R. Yueming, Q. Hui, Z. Shijun, Preparation of PTFE microporous membrane and its application in medical and health field, N. Chem. Mater. 50 (8) (2022) 263–266.
- [26] J.W. Martin, S.A. Mabury, K.R. Solomon, D.C. Muir, Progress toward understanding the bioaccumulation of perfluorinated alkyl acids, Environ. Toxicol. Chem. 32 (11) (2013) 2421–2423.
- [27] S. Haider, J.A. Lie, A. Lindbråthen, M.-B. Hägg, Pilot–scale production of carbon hollow fiber membranes from regenerated cellulose precursor-part I: optimal conditions for precursor preparation, Membranes 8 (4) (2018) 105.
- [28] G. Song, S.H. Kim, B.T.D. Nguyen, J.F. Kim, Fabrication of polymethylpentene (PMP) membranes using nonsolvent-thermally-induced phase separation (N-TIPS) method, Membrane Journal 34 (4) (2024) 216–223.
- [29] F. Burn, S. Ciocan, N. Mendez Carmona, M. Berner, J. Sourdon, T.P. Carrel, H. T. Tevaearai Stahel, S.L. Longnus, Oxygen-transfer performance of a newly designed, very low-volume membrane oxygenator, Interact. Cardiovasc. Thorac. Surg. 21 (3) (2015) 352–358.
- [30] L.J. Jones, R.P. Haugland, V.L. Singer, Development and characterization of the NanoOrange® protein quantitation assay: a fluorescence-based assay of proteins in solution, Biotechniques 34 (4) (2003) 850–861.
- [31] A. Ahmad, M. Zainuddin, M. Shah Buddin, Z. Mohd Shafie, Poly (4-methyl-1-pentene) membrane for CO2 separation: performance comparison of dense and anisotropic membrane, Arabian J. Sci. Eng. 48 (7) (2023) 8325–8338.
- [32] D. Kim, B.T.D. Nguyen, S.H. Kim, J. Kim, J.F. Kim, New Sherwood correlations for hollow fiber membrane contactor modules: Comparison of porous and nonporous asymmetric membranes, J. Membr. Sci. 723 (2025) 123939.
- [33] I.O.f. Standardization, ISO 10993-5: Biological Evaluation of Medical Devices Part 5: Tests for in Vitro Cytotoxicity (10993-5:2009 (E)), International Organization for Standardization, Switzerland, 2009.